Current-Line Oriented Pore Formation in n-InP Anodized in KOH

N. Quill[1,2], R. P. Lynch[1,2], C. O'Dwyer[3,4], D. N. Buckley[1,2]

[1]*Department of Physics and Energy, University of Limerick, Limerick Ireland*
[2]*Materials and Surface Science Institute, University of Limerick, Limerick Ireland*
[3]*Applied Nanoscience Group, Department of Chemistry, University College Cork, Cork Ireland*
[4]*Micro & Nanoelectronics Centre, Tyndall National Institute, Lee Maltings, Cork, Ireland*

Electrochemically formed pores in InP in KOH switch from being crystallographically oriented (CO) to being current-line oriented (CLO) above a specific potential in both 17 mol dm^{-3} and 2.5 mol dm^{-3} KOH at a temperature of 10°C. The CLO pores formed in KOH have roughly elliptical cross sections, and are wider along the $<01\bar{1}>$ than along the perpendicular <011> direction. The CLO pores can form only when a critical porosity is reached and their formation marks the transition from porous to planar etching. Many of the features of pore formation are explained by evoking the effect that both temperature and electrolyte concentration can have on the effective diffusion length of holes at the semiconductor-solution interface.

INTRODUCTION

The electrochemical formation of porous semiconductors has received considerable research attention[1-5]. While much of the work has focused primarily on porous silicon[1, 4], a wide range of porous structures have also been formed in III-V compounds[3, 5, 6]. In InP, two distinct pore morphologies can be identified: crystallographically oriented (CO) pores[5, 7] and current-line oriented (CLO) pores[8, 9]. CO pores grow along the <111>A crystallographic directions[10] and CLO pores grow in the direction of the current flow through the electrode.

Many models have been proposed[1, 2, 11-14] to account for the formation of porous semiconductors. However, despite the numerous attempts at explaining porous semiconductor phenomena, no general model has been able to account for the wide range of structures produced by the variation of electrolyte type and concentration[15, 16], substrate type[17], orientation[18] and doping density[19].

Switching between CO and CLO pore morphologies allows the creation of complex three-dimensional structures with varying refractive index which may be useful in the formation of Bragg filters, waveguides or photonic crystals[20-22]. The pore walls can be thinned to only a few nm during CLO pore etching in KOH. This would be expected to lead to quantum confinement effects in the remaining InP material[23-25]. The variety of pore morphologies that can be produced by the anodic etching of InP in KOH makes it a potentially interesting process for the fabrication of a range of complex, tailored nano- and mesostructures.

We have previously reported the formation of CO pores in InP electrodes anodized in >2 mol dm^{-3} KOH[5, 16]. These pores were shown to emerge from pits in the electrode

surface[26] and etch along the <111>A crystallographic directions[10]. Here, we detail the formation of CLO pores by the anodisation of InP in KOH. The formation of these structures, and the conditions under which they form will be shown to support a model for the formation of porous semiconductors based on a three-step mechanism of charge transfer with the electrolyte.

EXPERIMENTAL

The working electrode consisted of polished (100)-oriented monocrystalline sulphur doped ($n = 5 – 5.6 \times 10^{18}$ cm^{-3}) n-InP. An ohmic contact was made to the back of the InP electrode and the back and sides of the electrode were isolated electrically from the electrolyte by means of a suitable varnish. The electrode area was typically 0.2 cm^2. The etch pit density of all samples used was less than 5×10^3 cm^{-2}. Anodisation was typically carried out in aqueous KOH electrolytes at a concentration of 17 mol dm^{-3} at 10°C, but a range of other concentrations and temperatures were also used. A conventional three-electrode cell configuration was used employing a platinum counter electrode and a saturated calomel reference electrode (SCE) to which all potentials were referenced. Prior to immersion in the electrolyte, the working electrode was dipped in an etchant (3:1:1 H_2SO_4:H_2O_2:H_2O) for 4 minutes and then rinsed in deionised water. All electrochemical experiments were carried out in the absence of light. The temperature was held constant by a thermostatic water bath connected to a water jacket cell in which the experiments were carried out.

A CH Instruments Model 650A Electrochemical Workstation was employed for cell parameter control and for data acquisition. Cleaved {011} cross-sections and the (100) surfaces were examined using a Hitachi S-4800 field-emission scanning electron microscope (SEM) operating at 5 kV.

RESULTS AND DISCUSSION

Porous Layer Morphology in 17 mol dm^{-3} KOH

Porous InP is typically formed in HCl electrolytes and exhibits both CO and CLO pore morphologies[9]. In KOH, typically only CO pore growth is observed [5, 16]. The porous etching of InP occurs in KOH concentrations ranging from about 2 mol dm^{-3} to about 17 mol dm^{-3} [27]. While CO pore growth is observed over this entire concentration range, CLO pore growth is observed to occur only in both the highest, and lowest KOH concentrations in which pore growth occurs (~ 2 to 17 mol dm^{-3}), at temperatures at or below 10°C.

A series of linear-sweep voltammograms (LSVs) of InP electrodes anodised in 17 mol dm^{-3} KOH at a range of temperatures are shown in Fig. 1. With the exception of the sample anodized at 10°C, these LSVs are typical of what is seen for the anodization of InP in KOH[27]. The LSVs typically exhibit 2 current peaks, where the second peak indicates the cessation of porous layer etching. This second peak is typically followed by a continuous decay in current. This decay in current is not observed in the LSV acquired at 10°C.

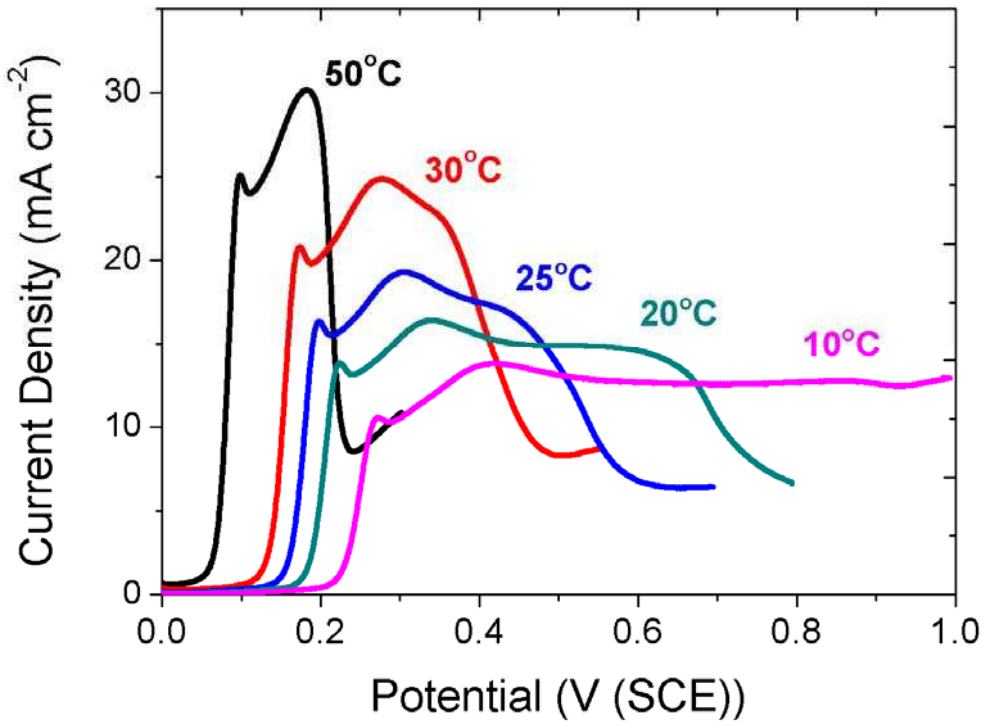

Figure 1. A series of LSVs of InP electrodes anodised in 17 mol dm^{-3} KOH at a scan rate of 2.5 mV s^{-1} at a range of temperatures.

A series of SEM micrographs of porous layers which were formed by linear potential sweeps (LPSs) at different temperatures are shown in Fig. 2. Figure 2a shows the porous layer formed at 40°C. The layer shows a CO pore structure throughout its entire thickness. A similar CO pore structure can be seen in the sample formed at 25°C (Fig. 2b). The porous layer formed at 10°C (Fig. 2c) initially shows a CO morphology, with wider pores than those formed at higher temperatures. As the layer thickened however, it began to switch to a CLO pore morphology which can be seen at the bottom of Fig. 2c. The CO pores have typical widths of ~40 nm and pore wall thicknesses of ~25 nm. The CLO pores, by comparison, have typical widths >100 nm with corresponding pore wall thicknesses of ~10 nm or less (measured on the (011) plane).

Potentiostatic Pore Formation in 17 mol dm^{-3} KOH

A series of current-time plots of InP electrodes potentiostatically anodized in 17 mol dm^{-3} KOH at 10°C at a range of potentials are shown in Fig. 3. The sample anodized at 0.4 V exhibited a gradual increase in current up to a peak, which is indicative of a progressive nucleation of etching sites (surface pits). All other samples exhibited an initially large current density which decayed rapidly, indicating an instantaneous nucleation of etching sites (surface pits) across the electrode surface.

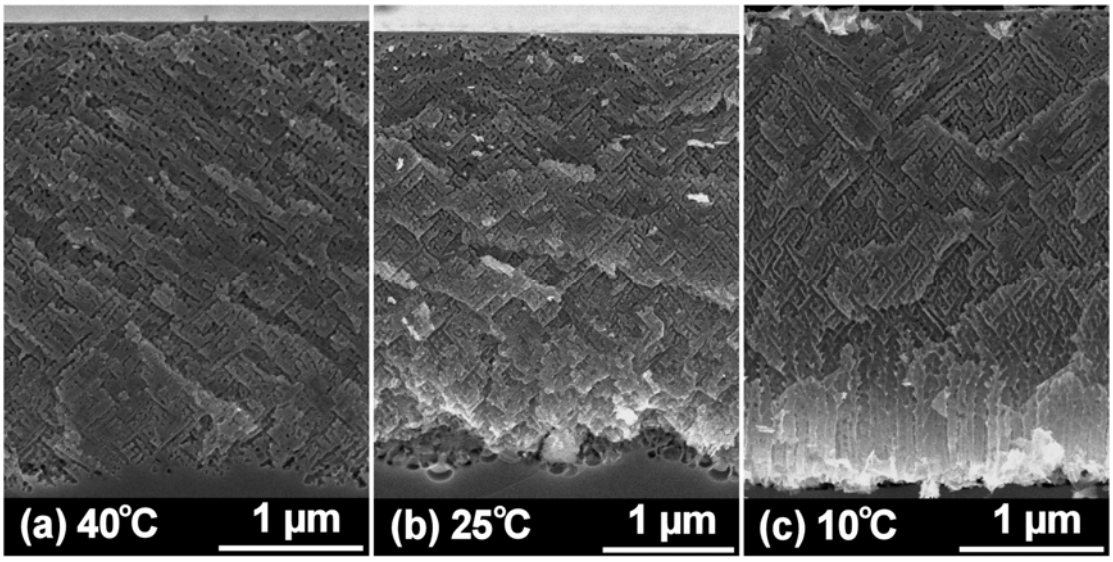

Figure 2. Cross-sectional SEM micrographs of the (011) planes of InP electrodes anodised in 17 mol dm^{-3} KOH by LPS at a scan rate of 2.5 mV s^{-1} at a range of temperatures. Images (a), (b) and (c) show porous layers formed at 40°C, 25°C and 10°C respectively.

A series of SEM micrographs of the porous layers formed potentiostatically are shown in Fig. 4. Below 0.6 V, CO pore growth was observed. Figure 4a shows the layer formed at 0.6 V. The layer initially shows a CO pore morphology which develops into a CLO pore morphology as it thickens. As the potential was increased, pore walls became smoother and thinner. This can be seen in Fig. 4b which shows the sample anodized at 0.9 V which exhibited a short CO section and exhibits uniform CLO pore growth (smooth pore walls) throughout the thickness of the layer. Figure 4c shows the sample anodized at 1.0 V. Again, a short CO nucleation phase rapidly gives way to CLO pores. The pore walls are again much smoother than those formed at lower potentials, and the measured pore widths show the least uniformity among all samples investigated. As the pores grow deeper into the substrate, they appear to widen continuously until pore walls and individual pores become difficult to distinguish.

CLO Pore Shape

A series of SEM micrographs of the (100) surface of an InP electrode anodised at 0.9 V are shown in Fig. 5. Figure 5a shows that the electrode surface contains a high density of surface pits from which porous etching commences[26, 28]. Figure 5b shows where a portion of the electrode surface was fractured, which opened up a region of the underlying CLO pore structure allowing the CLO pore cross section to be examined. Figure 5c shows a higher magnification view of the CLO pore cross section. It is clear that the pore walls have a curved shape and do not appear to be bounded by any particular crystallographic plane. The majority of the pores seem to have an approximately elliptical cross section, with the major axis of the ellipse parallel to the $<01\bar{1}>$ direction. Multiple ‘pore merging’ events can be seen throughout the image, in which two adjacent pores join together along the $<01\bar{1}>$ direction to form a single larger pore.

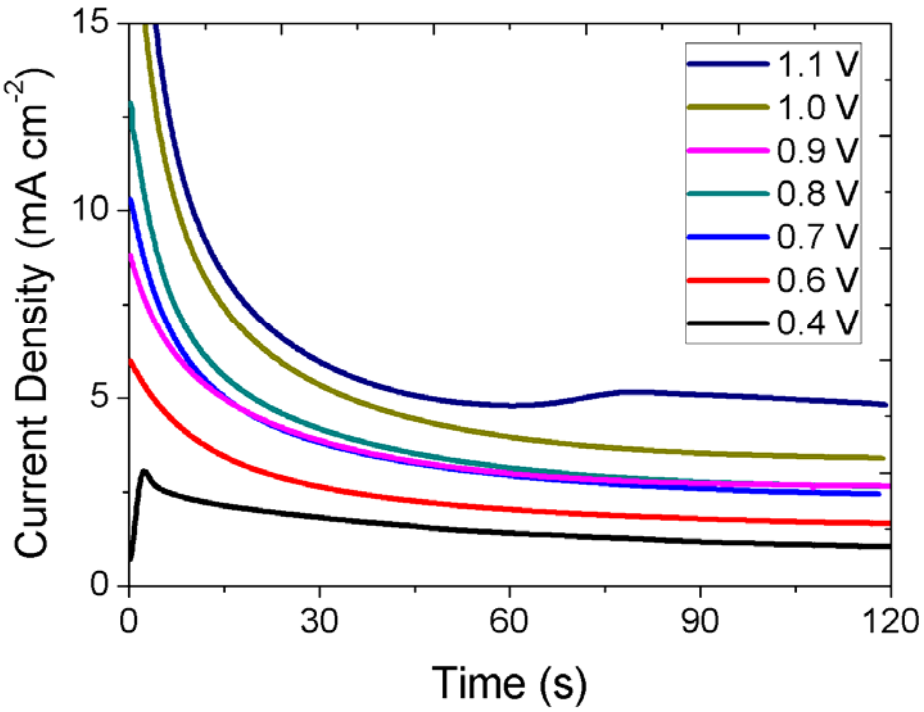

Figure 3. A series of current-time plots of InP electrodes anodised at constant potentials in 17 mol dm^{-3} KOH at 10°C. The anodisation potentials range from 0.4 to 1.1 V.

The pore width measured along the $<01\bar{1}>$ direction is on average 2.5 times greater than the pore width measured along the <011> direction. This suggests that any pore observed in this (100) cross section may be the result of the amalgamation of two or more pores. Typically, for the InP/KOH pore etching system, if a growing pore tip approaches another pore, etching stops for that pore tip due to the lack of carrier supply caused by the overlap of the depletion regions surrounding each pore. Passivated pore walls are a requirement for anisotropic pore etching.

Formation of CLO Pores at other KOH Concentrations

When samples are anodized at high potentials (>0.8 V) and at low temperatures at concentrations below 17 mol dm^{-3}, true CLO pores are typically not observed. Fig. 6a shows an SEM micrograph of a porous layer formed at 0.9 V at 10°C in 5 mol dm^{-3} KOH. While the pores are clearly deviating from their preferential growth directions, they still regularly attempt to branch out as they grow deeper into the substrate and appear closer in structure to CO pores than CLO pores. This is typical of what is seen at the majority of KOH concentrations. Fig. 6b shows an SEM micrograph of a porous layer formed at 0.8 V in 2.5 mol dm^{-3} KOH at 10°C. Here a more CLO pore morphology is observed.

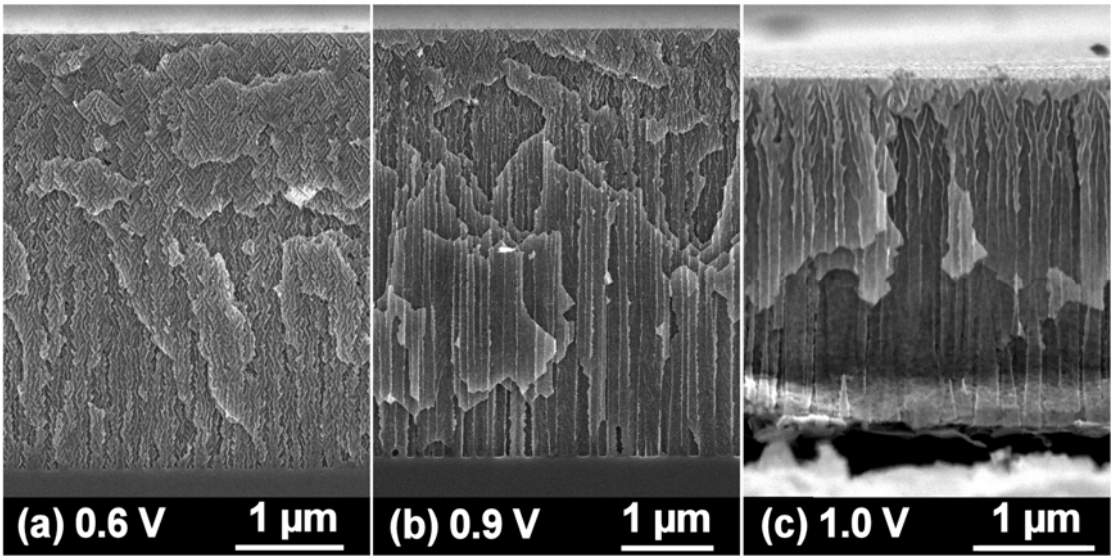

Figure 4. Cross sectional SEM micrographs of the (011) planes of InP electrodes, each anodised at a different constant potential in 17 mol dm^{-3} KOH at 10°C. The electrodes were anodised at (a) 0.6 V, (b) 0.9 V and (c) 1.0 V.

CLO pores can form at a sufficiently high potential, below room temperature in both 2.5 mol dm^{-3} and 17 mol dm^{-3} KOH (the lowest and highest concentrations in which porous etching occurs, respectively). It has been shown elsewhere[27] that pore width and associated porosity are higher when pores are formed at lower temperatures and in either high or low KOH concentrations. This suggests that CLO pores can only form at high potentials, after a critical porosity has been achieved. It has previously been proposed[29] that branched CO pore growth initially occurs due to inhomogeneous pore distribution. If, by some mechanism, an increase in pore width or pore density occurred, the resulting high density of pores would lead to increasingly thin pore walls which would become effectively passivated due to depletion. This would prevent pore branching and maintain pore growth along the direction of the source of holes. This model seems particularly relevant to the formation of CLO pores in InP etched in KOH since CLO pore growth is typically observed for parameters where pores are expected to be at their widest and pore walls at their thinnest.

Three-step Charge Transfer Model

The general features of CLO pore formation, as well as the 'pore merging' phenomenon can be understood in the framework of a qualitative model for the electrochemical formation of porosity in semiconductors based on the charge transfer between the semiconductor and the electrolyte. This model was proposed to account for the variation of pore width with carrier concentration, temperature and KOH concentration[27, 30]. Charge transfer in this model involves three main steps. The first step is the supply of holes to the pore tip, which is necessary for etching to take place. This is likely to occur only at the pore tips in the region of enhanced electric field due to the surface curvature of the tips[4], and the dominant breakdown mechanism is likely to be tunnelling[31, 32]. For the formation of CO pores, this hole supply is likely to be the rate limiting step.

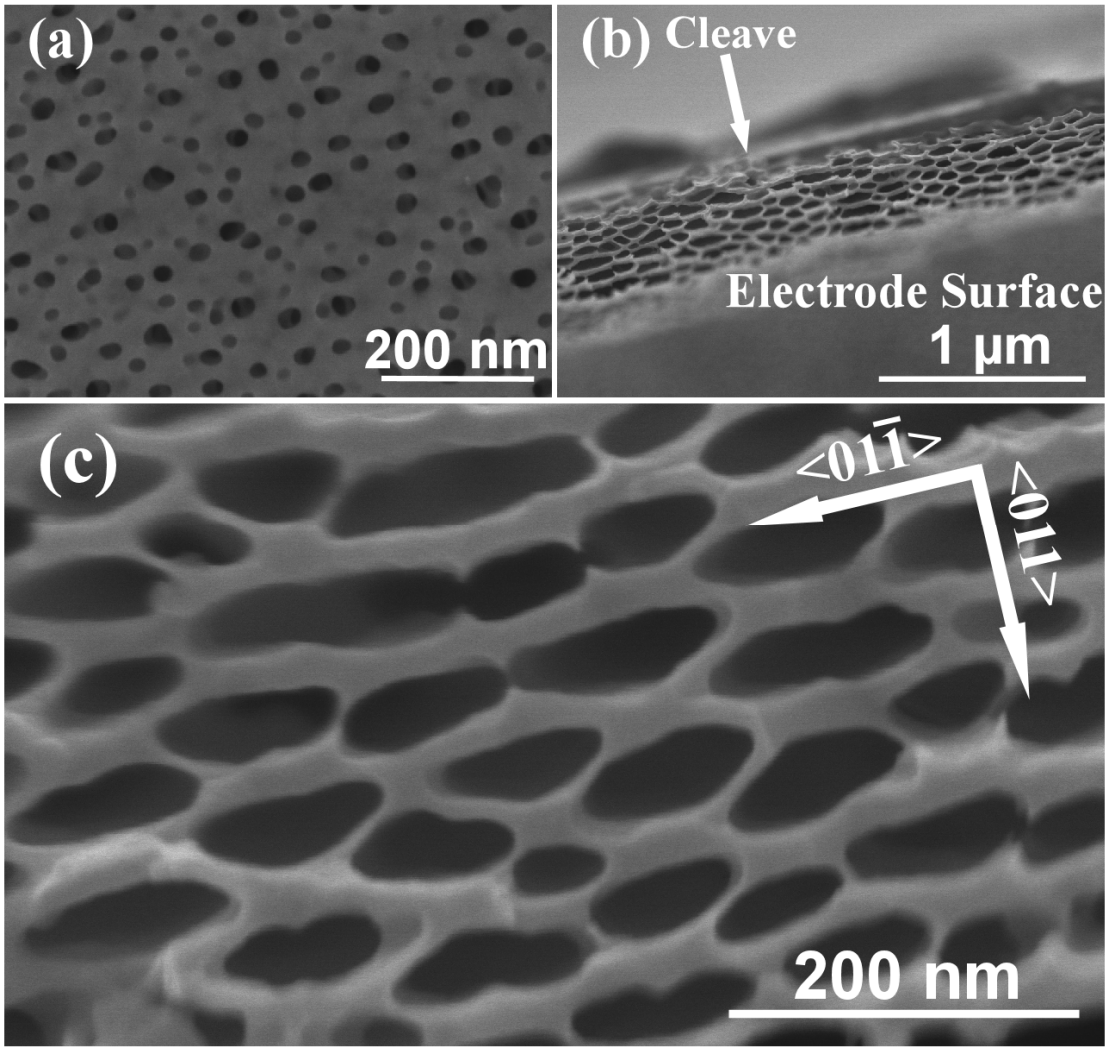

Figure 5. SEM micrographs of the (100) plane of an InP electrode anodised in 17 mol dm^{-3} KOH at 10^{o}C at a constant potential of 0.9 V. Image (a) shows the typical electrode surface, image (b) shows where a portion of the surface was removed during sample cleavage, revealing a window on the CLO pore (100) cross section (perpendicular to pore growth direction), which is shown at a higher magnification in image (c). The inset in (c) shows the crystallographic orientation of all of the images.

Holes which appear at the pore tip have some time to diffuse through the valance band and surface states of the semiconductor before being annihilated by an electron injected from the active species in solution. Hole diffusion and hole annihilation are the second and third steps in the charge transfer, respectively. While the rate at which CO pore etching occurs would not be affected by these two steps, the spatial extent of the reaction, and hence, the width of the pores would be affected. As in the model developed by Zhang[4], the minimum pore width is determined primarily by the width of the region of enhanced electric field that is present at the pore tip. Since the region surrounding the pore tip is depleted of carriers, any carrier that arrives at the pore tip is most likely due to tunnelling. This is only likely near the pore tip where the electric field is enhanced.

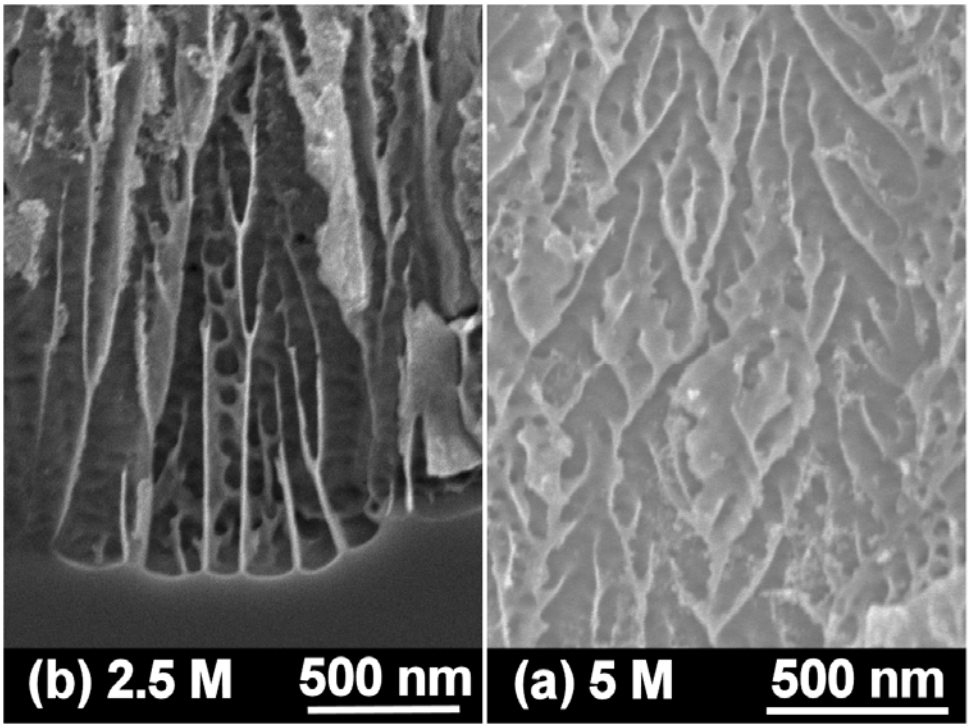

Figure 6. Cross sectional SEM micrographs of the (011) planes of InP electrodes anodised at 10^{o}C in (a) 5 mol dm^{-3} KOH at a constant potential of 0.9 V and (b) 2.5 mol dm^{-3} KOH at a constant potential of 0.8 V. Purely CLO pores are shown in image (b) while partially CO pores can be seen in image (a).

If holes arriving at the pore tip instantly take part in the electrochemical reaction, the measured pore width would be determined exclusively by the ratio between the width of the depletion layer and the curvature of the pore tip[4]. However, if the holes have some time to diffuse away from this region, then wider pores would be observed. The pore width then is determined by three factors; (i) the ratio of the width of the depletion layer to the radius of curvature of the pore tip, (ii) the diffusion rate of holes at the semiconductor surface and (iii) the kinetics of the electrochemical reaction (which determine how long a hole will exist on the surface before being annihilated). This model explains the variation of pore width with both temperature and KOH concentration that is observed for CO pore formation in KOH[27]. Figure 7 shows a schematic, illustrating the three important processes in the model.

When this model was applied to CO pore growth, it was assumed that hole supply across the depletion region of the semiconductor was rate limiting. At higher potentials, the rate of hole supply will increase and eventually may no longer be rate limiting. This potential will be reached sooner under conditions where the rate of hole annihilation by the electrochemical reaction is reduced. This is likely the case at low temperature and at both high and low KOH concentrations due to kinetic considerations. These conditions would result in an abundance of holes at the pore tips and a large hole diffusion length at the interface. This should result in planar etching, as carriers would be available at all points on the electrode surface, and etching could take place everywhere.

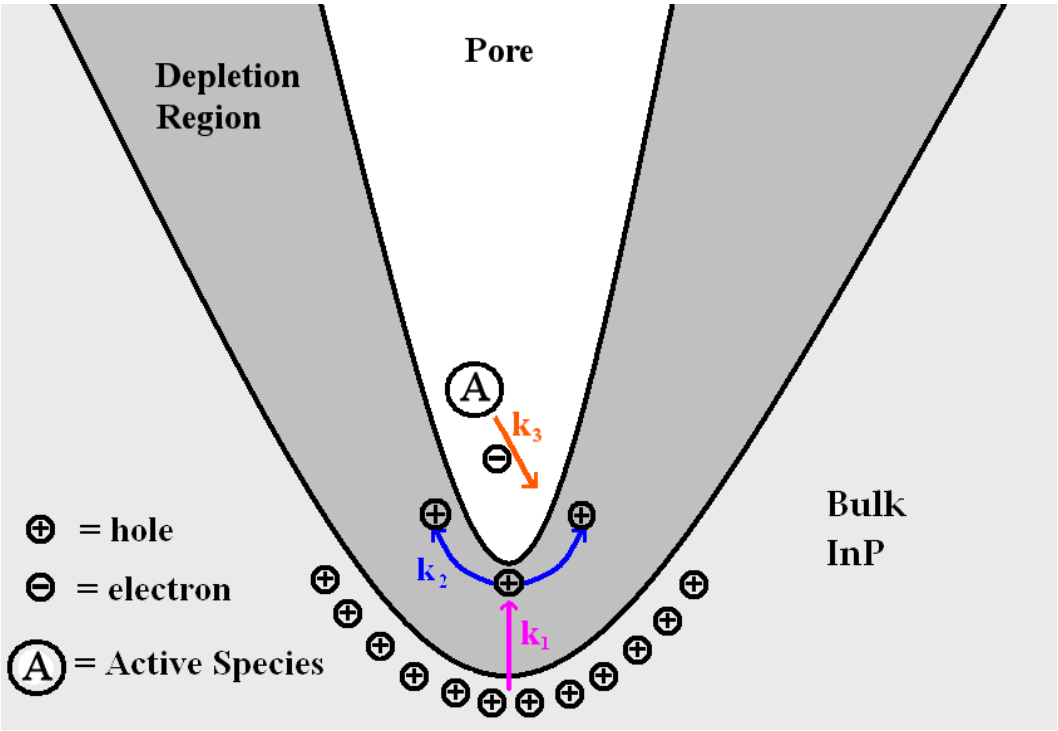

Figure 7. Schematic of the three-step charge transfer mechanism. k_1 represents the rate at which holes are supplied to the pore tip, k_2 represents the characteristic diffusion rate of holes at the semiconductor/electrolyte interface and k_3 represents the rate at which the active species in solution captures holes from (injects electrons into) the semiconductor.

With the preceding arguments in mind, consider the situation for CLO pore formation in KOH. For CLO pores to form in any electrolyte, large overpotentials are necessary i.e. it is necessary to increase the rate of hole supply at the pore tip. To achieve CLO pore growth in KOH, it is also necessary to use extreme electrolyte concentrations and to reduce the temperature of the electrolyte, thus limiting the rate of hole capture by the electrochemical reaction. From the arguments in the previous paragraph, these conditions are exactly what is needed to achieve planar etching.

It could be argued then, that CLO pore growth marks the transition between a dissolution process dictated by the supply of holes at the pore tip (CO pore etching), and a dissolution process dictated by the rate of electron injection of holes by the electrolyte (planar etching). As holes become more abundant at the interface, pores can widen continuously until they come into contact with another pore. This leads to the wide pores and very thin pore walls seen for CLO pores. A further increase in hole availability would result in planar etching. Evidence of this behaviour was seen in the experiments which formed CLO pore layers potentiostatically. As the potential was increased, pore walls became smoother and thinner. Between 0.9 V and 1.0 V, the pore walls became very thin, and sometimes were found to be removed altogether. This ‘pore merging’ phenomenon is visible in Fig. 5c. At potentials of 1.1 V and above, no porous layer was observed. Instead, a smooth InP surface was seen in SEM images (i.e. planar etching occurred).

CONCLUSIONS

The formation of CLO pores occurs between 0.6 and 1.0 V at 10^{o}C in both 2.5 mol dm^{-3} and 17 mol dm^{-3} KOH. CLO pores were formed when pore width and porosity were at their highest. This may indicate that they formed simply as a result of the high packing density of the pores under these conditions. For CLO pores formed in 17 mol dm^{-3} KOH, at 0.9 V and above the pore walls began to dissolve. At 1.1 V and above, planar etching occurred. The pore cross section was approximately elliptical, with the major axis of the ellipse being parallel to the $<01\bar{1}>$ direction.

A qualitative model based on a three-step mechanism of charge transfer between semiconductor and electrolyte was used to explain the formation of CLO pores. It was proposed that CLO pores mark the transition from CO etching to planar etching. As holes become more and more abundant at the pore tip, and the rate of hole capture by the electrochemical reaction decreases, the pores begin to widen continuously. These widening pores eventually reach a packing density so high that branching is impossible and holes are available only in the direction of the bulk InP, leading to CLO pore growth. As the abundance of holes at the semiconductor/electrolyte interface reaches a critical value, planar etching begins to occur.

ACKNOWLEDGEMENTS

Two of the authors, R.P. Lynch and N. Quill, would like to thank the Irish Research Council for Science Engineering and Technology for postgraduate scholarships to perform this research.

REFERENCES

1. R. L. Smith and S. D. Collins, *Journal of Applied Physics*, **71**, R1 (1992).
2. M. I. J. Beale, J. D. Benjamin, M. J. Uren, N. G. Chew and A. G. Cullis, *Journal of Crystal Growth*, **73**, 622 (1985).
3. H. Föll, J. Carstensen, S. Langa, M. Christophersen and I. M. Tiginyanu, *physica status solidi (a)*, **197**, 61 (2003).
4. X. G. Zhang, *Journal of The Electrochemical Society*, **151**, C69 (2004).
5. C. O'Dwyer, D. N. Buckley, D. Sutton and S. B. Newcomb, *Journal of The Electrochemical Society*, **153**, G1039 (2006).
6. H. Foll, J. Cartensen and S. Frey, *Journal of Nanomaterials*, 1 (2006).
7. E. Spiecker, M. Rudel, W. Jäger, M. Leisner and H. Föll, *physica status solidi (a)*, **202**, 2843 (2005).
8. A. Hamamatsu, C. Kaneshiro, H. Fujikura and H. Hasegawa, *Journal of Electroanalytical Chemistry*, **473**, 223 (1999).
9. S. Langa, I. M. Tiginyanu, J. Carstensen, M. Christophersen and H. Foll, *Electrochemical and Solid-State Letters*, **3**, 514 (2000).
10. R. P. Lynch, C. O'Dwyer, D. Sutton, S. B. Newcomb and D. N. Buckley, *ECS Transactions*, **6**, 355 (2007).
11. V. Lehmann and H. Foll, *Journal of The Electrochemical Society*, **137**, 653 (1990).
12. V. Lehmann and U. Gosele, *Applied Physics Letters*, **58**, 856 (1991).

13. T. Unagami, *Journal of The Electrochemical Society*, **127**, 476 (1980).
14. H. Föll, M. Christophersen, J. Carstensen and G. Hasse, *Physica status solidi (a)*, **182**, 7 (2000).
15. P. Schmuki, J. Fraser, C. M. Vitus, M. J. Graham and H. S. Isaacs, *Journal of The Electrochemical Society*, **143**, 3316 (1996).
16. R. P. Lynch, C. O'Dwyer, D. N. Buckley, D. Sutton and S. Newcomb, *ECS Transactions*, **2**, 131 (2006).
17. M. Christophersen, J. Carstensen, A. Feuerhake and H. Föll, *Materials Science and Engineering B*, **69-70**, 194 (2000).
18. S. Ronnebeck, J. Carstensen, S. Ottow and H. Foll, *Electrochemical and Solid-State Letters*, **2**, 126 (1999).
19. P. Schmuki, L. E. Erickson, D. J. Lockwood, J. W. Fraser, G. Champion and H. J. Labbe, *Applied Physics Letters*, **72**, 1039 (1998).
20. S. Langa, S. Frey, J. Carstensen, H. Foll, I. M. Tiginyanu, M. Hermann and G. Bottger, *Electrochemical and Solid-State Letters*, **8**, C30 (2005).
21. S. Langa, M. Christophersen, J. Carstensen, I. M. Tiginyanu and H. Föll, *physica status solidi (a)*, **197**, 77 (2003).
22. H. Tsuchiya, M. Hueppe, T. Djenizian and P. Schmuki, *Surface Science*, **547**, 268 (2003).
23. T. Takizawa, S. Arai and M. Nakahara, *Japanese Journal of Applied Physics*, **33**, L643 (1994).
24. A. Liu and C. Duan, *Solid-State Electronics*, **45**, 2089 (2001).
25. P. Hidalgo, J. Piqueras, L. Sirbu and I. M. Tiginyanu, *Semiconductor Science and Technology*, **20**, 1179 (2005).
26. C. O'Dwyer, D. N. Buckley, D. Sutton, M. Serantoni and S. B. Newcomb, *Journal of The Electrochemical Society*, **154**, H78 (2007).
27. N. Quill, R. P. Lynch, C. O'Dwyer and D. N. Buckley, ***this volume*** (2012).
28. P. Schmuki, U. Schlierf, T. Herrmann and G. Champion, *Electrochimica Acta*, **48**, 1301 (2003).
29. S. Frey, M. Kemell, J. Carstensen, S. Langa and H. Föll, *physica status solidi (a)*, **202**, 1369 (2005).
30. R. P. Lynch, N. Quill, C. O'Dwyer and D. N. Buckley, ***this volume*** (2012).
31. V. Lehmann, R. Stengl and A. Luigart, *Materials Science and Engineering: B*, **69–70**, 11 (2000).
32. J. C. Tranchart, J. Hollan and R. Memming, *Journal of The Electrochemical Society*, **125**, 1185 (1978).